Energetics of bent carbon nanotubes

V. Meunier, L. Henrard, and Ph. Lambin
Département de Physique, Facultés Universitaires Notre-Dame de la Paix, 61 Rue de Bruxelles, B 5000 Namur, Belgium
(Received 11 June 1997)

Several junctions between different nanotubes have been constructed which preserve the C sp^2 honeycomb lattice with the sole insertion of a pentagon and a heptagon. This construction bends the structure at an angle that depends on the distance between the pentagon and heptagon. The atomic structure of these systems was optimized with empirical interatomic potentials. The nanotubes on both sides of the junctions were treated as infinitely long. Local $\sigma+\pi$ electron densities of states were computed locally in the interfacial region with a tight-binding Hamiltonian. From this, the electron energy of the junctions was computed and compared to that of the separated nanotubes. It is found that the energy of a pentagon-heptagon defect in the graphitic tubular network is around 6 eV. [S0163-1829(98)04504-4]

I. INTRODUCTION

The prospect for potential applications of carbon nanotubes has become a field of growing interest.[1–4] In this respect, connecting two different nanotubes offers the possibility to build elementary logical devices at the nanometer scale.[1,2] For that reason, the electronic properties of a junction between two different nanotubes have been investigated with some details from the theoretical point of view.[5–10] Since the electronic structure of a nanotube depends on its atomic structure,[11–13] the latter has to be changed at the junction between two different systems. As predicted theoretically, connecting two nanotubes with different diameters and helicities can be realized by inserting a pentagon and a heptagon in the otherwise perfect honeycomb lattice.[14] A large variety of connections can be realized in this way, depending on the relative positions of the two defects.[7,15] When the pentagon and heptagon are aligned along a side, straight connections can be realized.[7,8] Moving the two defects around the nanotube changes the structure and bends it at an angle that varies with the distance between the odd-membered rings. Adjacent defects lead to a small-angle bent,[6] while the diametrically opposed pentagon-heptagon give a large angle ($\sim 36°$). By repeating the insertion of a pentagon-heptagon pair at regular intervals, toroidal structures[16] and helicoidal coiled nanotubes[17] can be generated.

On the experimental side, there is no direct observation of pentagons and heptagons in carbon nanotubes, although their presence is highly suspected in several instances.[18] Pentagons are most likely present in the hemispheric caps that terminate a carbon nanotube, leading to specific effects in scanning tunneling microscopy and spectroscopy,[19] whereas the heptagons can explain how a conelike structure transforms into a straight cylinder.[20] In addition, regular coiled nanotubes have been produced,[21] in which high-resolution electron microscopy and diffraction studies revealed sharp bends between straight portions.[22] The dozen layers which the coils are composed of bend coherently at angles that have been determined to be $\sim 30°$.[23] A pentagon and an heptagon located at diametrically opposed positions in each layer, or close to, easily explain this observation.[24]

In the pentagon-heptagon construction, it is not clear whether it is more favorable to have the two defects adjacent, or well separated. If the perturbation concerned the immediate neighborhood of the defects, adjacent pentagons and heptagons would have a lower energy since the pair affect the 8 surrounding hexagons, instead of 12 for two separated defects. It has been argued that a pentagon-heptagon pair is a dislocation, or a series of dislocations, whose energy increases with the logarithm of their distance to the free ends of the system.[15] The present paper is aimed at examining this energetic question from a microscopic point of view, by comparing the energies of a few nanotube connections realized with the pentagon-heptagon construction.

Several nanotube junctions were constructed, including straight connections of zigzag nanotubes, and both small- and large-angle junctions between two nanotubes of different helicities. The atomic structure of these systems was optimized with a simulated annealing technique based on empirical C-C potentials described in the next section. Local electron densities of states were computed on the optimized structures in which the nanotubes on both sides of the junctions were treated as semi-infinite. A tight-binding Hamiltonian that included both σ and π electrons was used. From this, the band-structure energy of the junctions was computed and compared to that of the isolated nanotubes. It is confirmed that the energy of a pentagon-heptagon defect in a graphitic nanotube is 5 eV typically, that is to say of the order of a C-C covalent bond as predicted by the dislocation theory. No definitive conclusion can be drawn to assign an attraction or a repulsion between the two odd-membered rings.

II. ATOMIC STRUCTURE OPTIMIZATION

Starting from a two-dimensional mapping, a joint can be realized between two tubules specified by the couples (L_1,M_1) and (L_2,M_2).[14,7] From this construction, an approximate configuration can be realized in three dimensions. We were at first interested in kneed junctions in which the pentagon and the heptagon are on opposite sites of the structure. This geometry imposes the constraint[25] $L_1L_2-L_1M_2-M_1L_2-2M_1M_2=0$ when $M_1\geqslant 0$ and $M_2\geqslant 0$, and[7] $L_1L_2+2L_1M_2-M_1L_2+M_1M_2=0$ when $M_1\geqslant 0$ and $M_2\leqslant 0$. We

TABLE I. Summary of results for nanotube junctions obtained by introducing a pentagon and a heptagon as indicated in the second column. The third column gives the angle of the optimized structure of the junctions. The fourth column lists the energy of the defect based on a $\sigma+\pi$ electronic calculation and the fifth column gives the defect energy given by the Tersoff potential.

Junction	5-7 positions	Angle (°)	ΔE_{bs} (eV)	ΔE_{Ter} (eV)
(6,4)/(8,−1)	opposite	34	7.7	2.45
(9,0)/(5,5)[a]	opposite	36	5.0	2.12
(10,0)/(6,6)[b]	opposite	36	5.4	2.13
(18,0)/(10,10)	opposite	36	7.8	2.81
(20,0)/(12,12)	opposite	39	5.0	2.60
(8,0)/(7,1)[c]	adjacent	12	4.7	1.41
(12,0)/(11,0)[d]	adjacent	0	5.5	1.56

[a]References 5,30.
[b]References 5,28.
[c]Reference 6.
[d]References 7,8.

constructed atomic clusters representing the junctions (6,4)/(8,−1), (9,0)/(5,5), (10,0)/(6,6), (18,0)/(10,10), and (20,0)/(12,12). The first system is a hybrid of two chiral nanotubes. By contrast the next four junctions connect zigzag to armchair nonchiral configurations. Our choice was lead by the fact that the (9,0)/(5,5)@(18,0)/(10,10) and (10,0)/(6,6)@(20,0)/(12,12) are possible models for bilayer junctions.

For the purpose of comparison, we also investigated two systems in which the defects were adjacent, namely, the (12,0)/(11,0) and (8,0)/(7,1) junctions. The first is a straight connection between two zigzag nanotubes where the axis of the pentagon-heptagon defect is parallel to the axis of the nanotubes. The 5-7 axis has been rotated in the second connection, a small-angle knee. All the nanotube connections listed in Table I were optimized with the same technique. Several of these connections, having already been considered in other works (see Table I), will not be described in detail here.

The starting atomic structures of the nanotube junctions were relaxed numerically with a simulated-annealing algorithm based on two different empirical potentials. The first one is a force-field model proposed recently by Borštnik *et al.*[26] For the purpose of checking the optimization process, the same annealing technique was used with the Tersoff potential using the Brenner parametrization.[27] The potential of Borštnik *et al.* is well adapted to fullerenes and related sp^2 carbon networks. It includes nearest-neighbor two-, three-, and four-body interactions accounting for bond stretching, bending, and torsion, respectively, plus next-nearest-neighbor nonbonding van der Waals interactions.[26] It was this potential that we used in our previous evaluations of the conformation of the (9,0)/(5,5) and (10,0)/(6,6) knees.[5,28] The Tersoff potential is a sum of nearest-neighbor pair interactions that are modulated by the local atomic environment.[29] This potential is implicitly a three-body potential. It has been widely used in a range of applications and, when applied with Brenner parameters, it reproduces well the nearest-neighbor length and binding energy of graphite and diamond.[27]

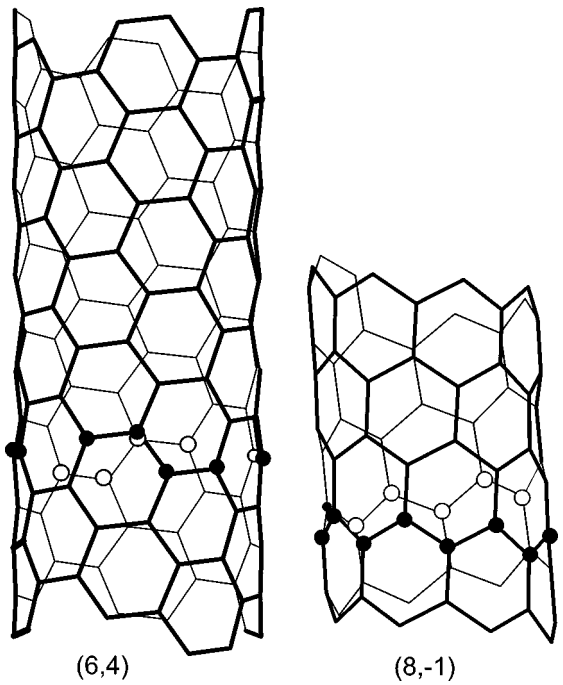

FIG. 1. Definition of a screw-cell of (6,4) (left) and (8,−1) (right) nanotubes. The helical pattern containing, respectively, 12 and 14 atoms per thread are shown by large circles. The symmetry operation is given by (τ,ψ) where τ is a translation along tubule axis and ψ is the rotation angle around tubule axis. For the (6,4) tubule, τ and ψ are respectively equal to 1.47 Å and 104°. For the (8,−1) tubule, the chiral parameters are 1.61 Å and 89°.

During the optimization process, the semi-infinite character of the tubules on both sides of the junction was simulated by considering three circumferencial rings at both ends of the cluster as being rigid entities. Thanks to the short range of the interactions, three rings suffice to simulate infinitely long tubules. A circumferential ring in the (L,M) nanotube is defined as an ensemble of $2L$ atoms closest as possible to a circumference [when $M<0$, the number of atoms required is $2(L+M)$]. This choice was inspired by the fact that for a chiral (L,M) nanotube, a number of $2L$ atoms [$2(L+M)$ when $M<0$] is sufficient to define a complete thread of screw. For instance, a ring of 12 (respectively, 14) atoms in the (6,4) [respectively, (8,-1)] tubules are shown in Fig. 1. In the case of achiral nanotubes, a zigzag ring of $2L$ carbons is used for the $(L,0)$ nanotube, and a series of L carbon pairs around a circumference defines a ring in the (L,L) configuration.

We first applied the potential of Borštnik *et al.*, which permits a reasonably fast numerical convergence to the optimum structure. The simulated annealing process was performed with a fixed connection table of the atoms, while decreasing the temperature gradually from 500 to 1 K. The optimized structure was then used as the input of a second simulated-annealing process with Tersoff potential, using a lower starting temperature. This refinement of the structure only leads to small changes of the coordinates.

The optimized structures of the bent nanotubes (6,4)/(8,−1) and (20,0)/(12,12) are presented in Fig. 2. The open circles in Fig. 2 show the two parts of the (6,4) and (8,−1) nanotubes that were kept rigid during the optimization. The rings at the bottom end were kept fixed in position, while the

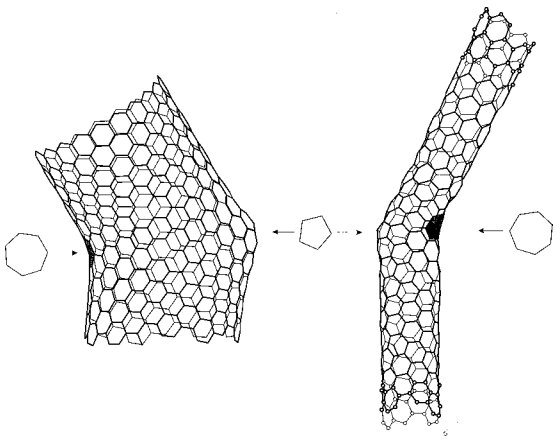

FIG. 2. Optimized structure of (20,0)/(12,12) and (6,4)/(8,−1) bent nanotubes using Borštnik *et al.* force-field potential in a simulated annealing Monte Carlo process. During the optimization process, the semi-infinite character of the tubules on both sides of the junction was simulated by considering three circumferencial rings at both ends of the cluster as being rigid entities. These atoms are explicitly shown by open circles on the figure for the junction (6,4)/(8,−1). The 3 times 12 atoms of the (6,4) tubule (bottom) were kept fixed in position whereas the 3 times 14 atoms of the (8,−1) tubule (top) could only move as a single entity. In both cases, the heptagon is opposite to the pentagon. The measured angle is slightly greater than the value expected with a two-dimensional graphene sheet construction. The first structure is bent at an angle of 39° and the second one has an angle of about 34°.

ones at the top could move rigidly. By doing so, the bending angle between the two nanotubes was optimized by the relaxation process. The average length of the bonds is 1.42 Å. This value increases slightly in the heptagon. The pentagon is planar and the heptagon is boat shaped to accommodate the negative curvature at the inner side of the knee. The bending angles in the optimized structures are 34° for the (6,4)/(8,−1) connection and 39° for the (20,0)/(12,12) system, respectively. As indicated in Table I for the other junctions, opposite pentagon-heptagon bend the structure to an angle that varies between these two values, which are significantly greater than the angle of 30° obtained with the two-dimensional Dunlap construction.[14] The structure of a cluster model of the (9,0)/(5,5) connection was also optimized by a semiempirical technique of quantum chemistry,[30] which led to the same 36° bending angle as here. The angle of the optimized structure of the (8,0)/(7,1) connection, with its adjacent pentagon-heptagon, is 12°. In closing this section, let us make a remark about the (20,0)/(12,12) structure illustrated in Fig. 2. As in giant fullerenes, rebonding the atoms around the pentagon so as to create an additional 5-7 pair leads to a much more ''round'' structure of the knee.[31] Except for having tested that it works, this possibility was not explored deeper.

III. ELECTRONIC PROPERTIES

The electronic properties of the nanotube connections were explored with a tight-binding Hamiltonian based on the four *s* and *p* valence orbitals. Only first-neighbor interactions were considered in the Slater-Koster description,[32] with parameters that were fitted to the band structure of graphite[33] ($\epsilon_s=-5.49$ eV, $\epsilon_p=0$, $H_{ss\sigma}=-4.80$, $H_{sp\sigma}=4.75$, $H_{pp\sigma}=4.39$, and $H_{pp\pi}=-2.56$ eV). Local electronic densities of states (DOS) were obtained by application of the recursion method.[34] By contrast with the one-orbital (π) approximation widely used in the present context,[10] the four-orbital DOS's depend on the detailed atomic structure and not only on the connection table of the atoms. These details, through the σ-π mixing brought about by the curvature of the carbon network, do not modify significantly the behavior of the DOS near the Fermi level, except for the case of ''metallic'' nanotubes (for which $L-M$ is a multiple of 3).[35] In fact, only the armchair (L,L) nanotubes are real conductors. All the other ''metallic'' nanotubes (in the sense of the mentioned rule) have a small gap at the Fermi level, which rapidly decreases with increasing diameter. This property does not show up within the simple one-orbital approximation but is clearly demonstrated with the four-orbital Hamiltonian.[35] This indicates that the rule mentioned previously is based on topological effects only. This also underlines the importance the relaxation process has on the electronic properties.

Calculations of the charge on the defect rings reveals an excess of electron on the pentagon (+0.40 electron) and a deficiency on the heptagon (−0.25 electron) for all the joints listed in Table I. This might be understood as a consequence of Hückel's rule which states that cyclic π-electron systems having 6, 10, ... , π electrons are the most stable ones. The five- and seven-membered rings of the junction will therefore tend to form a six-π-electron system by charge transfers to stabilize the defect.[36]

The electronic properties of the relaxed (6,4)/(8,−1) and (20,0)/(12,12) junctions are shown below. In both cases, the Fermi level E_F coincides with the atomic *p* level, taken as the zero of energy. Two long nanotubes were connected at both ends of the structures to avoid border effects. The recursion method leads to a continued-fraction expansion of the density of states as a function of the energy. In this work, 150 continued-fraction levels were used with a small imaginary part (0.02 eV) added to the energy to force the convergence. The drawback of this procedure is that rapid variations of the DOS, such as the band edges, are slightly smoothed out.

A. (6,4)/(8,−1) junction

This junction resembles the (8,0)/(7,1) system investigated by the Berkeley group.[6] Their (7,1) and our (8,−1) nanotubes are two enantiomers which should be ''metallic'' according to the $L-M$ rule. In fact, they are semiconductors with a small gap (0.10 eV). By comparison, the (6,4) nanotube is a moderate-gap semiconductor (0.90 eV). The (6,4)/(8,−1) junction is not truly a semiconductor-metallic joint, nor either is the (8,0)/(7,1).

The DOS of the two separate (6,4) and (8,−1) nanotubes are shown in the left-hand side of Fig. 3, together with the local DOS averaged on the two defect rings of the junction. The small band gap of the (8,−1) nanotube appears as a dip in a large plateau of states around E_F. The local DOS's across the junction are shown in the right-hand side of Fig. 3. These DOS's were averaged on successive circumferencial rings labeled (a)–(m), as defined above [12 atomic sites for the (6,4) nanotube, 14 atomic sites for the (8,−1) part, see

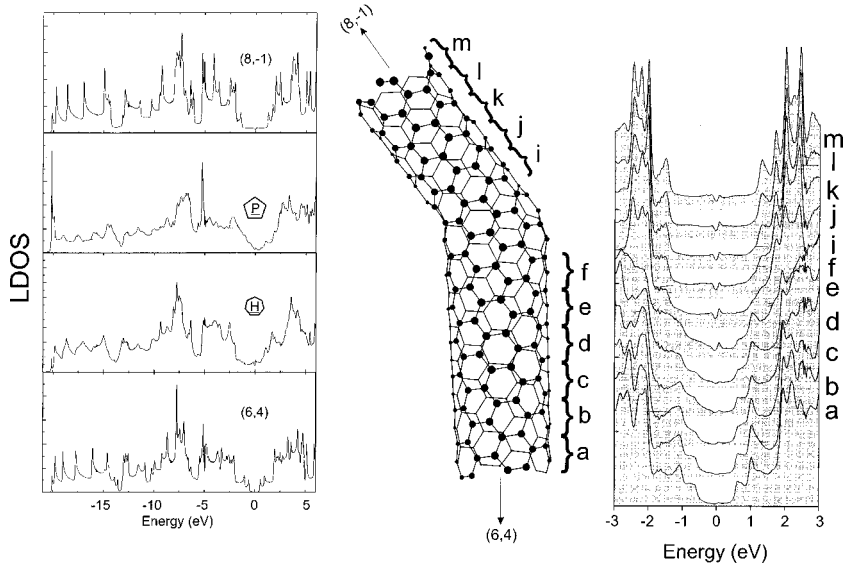

FIG. 3. LDOS of the (6,4)/(8,−1) bent nanotube formed with one single 5/7 defect. The left panel shows perfect (6,4) and (8,−1) nanotubes and LDOS averaged on pentagon and heptagon, respectively. The right panel presents LDOS from semiconductor to metallic nanotube. The LDOS is averaged on 12 (respectively, 14) sites in the (6,4) [respectively, (8,−1)] region. There is no evidence of oscillation at Fermi level for this chiral nanotubes junction. Although further investigations of the local density of states show some effect in the metallic part, there is no such clear effect as in the (20,0)/(12,12) junction.

also Fig. 1]. Above the interface, the plateau of states from the (8,−1) nanotube rapidly takes place on both sides of the small gap [curves (i)–(m)] that forms a small dip at E_F in all the curves. As with the (8,0)/(7,1) system,[6] states are induced in the band gap of the (6,4) semiconductor by the states of the (8,−1) nanotube. The density of these induced states decreases with increasing distance to the interface [curves (d)–(a)] but is still there in section a, located 20 Å below the interface.

B. (20,0)/(12,12) junction

This is a real semiconductor-metal hybrid. The (20,0) zigzag nanotube is a semiconductor with a gap of 0.30 eV, whereas the armchair (12,12) nanotube is a true metallic system. Figure 4 shows how the transition operate between the two types of systems when moving from the semiconductor to the metallic nanotube. In the metallic part, the DOS near E_F oscillates around the value of the plateau typical of the armchair nanotubes. This was already noted for the analog (10,0)/(6,6) connection.[5] This effect reflects the existence of standing waves generated by metallic Bloch states with wave vectors close to the Fermi wave vector k_F. These waves are evanescent in the zigzag (20,0) tubule because they fall within the semiconductor band gap. They are, therefore, reflected towards the metallic nanotube where their interference with the incoming states and form a standing wave. The period of the spatial oscillation of the local DOS so generated is around $2\pi/2k_F$, which is three times the distance between two circumferencial rings in the armchair tubules. (The Bravais period is two times that distance, but additional symmetry brought about by screw operations allows one to work in a double-sized first Brillouin zone.[35])

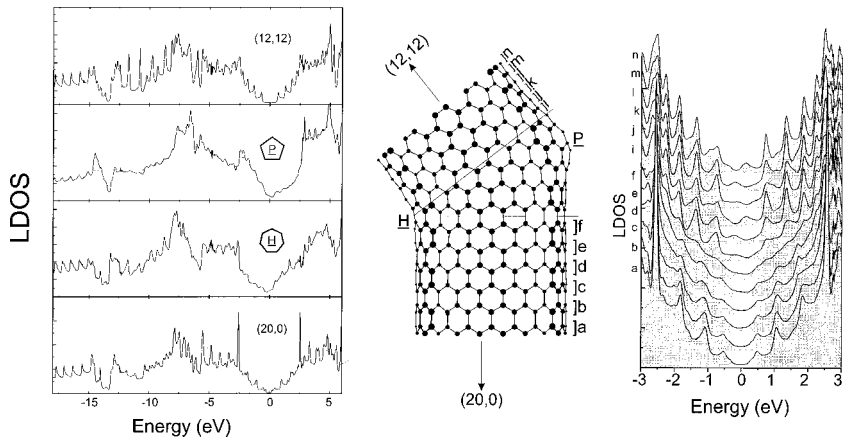

FIG. 4. LDOS of the (20,0)/(12,12) bent nanotube formed with one single 5/7 defect. The left panel shows perfect (20,0) and (12,12) nanotubes and LDOS averaged on pentagon and heptagon sites, respectively. The right panel presents LDOS from semiconductor to metallic nanotube. The oscillations around a plateau near the Fermi level in the metallic part are an evidence of the existence of standing waves which oscillate with a wave vector k_F and which do not propagate deeply in the semiconductor part of the heterostructure.

IV. ENERGY OF 5-7 DEFECT

In this last section, we discuss the energy of the defect which we evaluated from two different approaches. The first one is an electronic calculations and the other is based on the Tersoff potential. They are both a measure of the lack of stability of the bent nanotube versus straight, defect-free tubules.

A. Electronic energy of the defect

The tight-binding calculations referred to in the previous section allow us to evaluate the energy associated with the pentagon-heptagon defect. The electron band energy of the defect is computed from

$$\Delta E_{bs}=\sum_{i=1}^{N_{at}}\sum_{\mu=1}^{4}\int_{-\infty}^{E_F}(E-\varepsilon_{i\mu})\Delta n_{i\mu}(E)dE, \qquad (1)$$

where $\varepsilon_{i\mu}$ is the energy of the μth orbital centered on the ith atomic site and $\Delta n_{i\mu}(E)$ is the difference in the local DOS's on the site i between the joint and the perfect tubule. This supposes that the sites can clearly be identified as coming from one nanotube or the other, which causes no problem for the sections (a)–(f) and (d)–(n) illustrated in Figs. 3 and 4. The sites belonging to the intermediate region were attributed to both nanotubes with 50-50 %.

With the four-electron tight-binding Hamiltonian, we found $\Delta E_{bs} = 7.7$ eV in the case of $(6,4)/(8,-1)$ and 5.0 eV in the case of (20,0)/(12,12). The defect energies of the other junctions are given in Table I. The values obtained by this approach agree qualitatively with an estimation of the defect energy based on the dislocation point of view.[15] In contrast, the defect energy obtained by tight-binding calculations based on the sole π-orbital is too small by a factor of 4 to 10. For instance, the adjacent pentagon and heptagon in the (12,0)/(11.0) junction have an energy of 1.3 eV with the π-electron approximation,[8] to be compared with the present 5.5 value. A reason for this discrepancy has already been noticed that not all geometrical effects are taken into account with this one-orbital approximation.

The perturbation brought about by the pentagon-heptagon defect affects the electronic properties of the system in a relatively large neighborhood. This was already clear from the local densities of states shown in Figs. 4 and 3, and is also apparent from the variations of the electronic energy shown in Fig. 5 for the (10,0)/(6,6) joint. Whereas the convergence of the local energy [obtained from Eq. (1) by restricting the summation to those sites located at a given distance from the interface] is rapid on the metallic (6,6) side, the energy on the semiconductor (10,0) side is more deeply perturbed.

No systematic rule can be deduced from the data of ΔE_{bs} listed in Table I about a possible decrease of the defect energy that would favor adjacent pentagons and heptagons. The nanotubes involved in the $(6,4)/(8,-1)$ and (8,0)/(7,1) connections have nearly the same radii, but there is a clear lowering of energy in favor of the latter. In contrast, the (10,0)/(6,6) and (12,0)/(11,0) joints are very different but have roughly the same energy. The fact is that displacing the pentagon one step relative to the heptagon needs to rebond the all structure and therefore leads to a system which does not directly compare with the original one. The energy can increase or decrease as well. The absence of general trends reported here could result from the fact that the structural optimizations were not based on a minimization of the electronic energy but minimized the Tersoff potential instead.

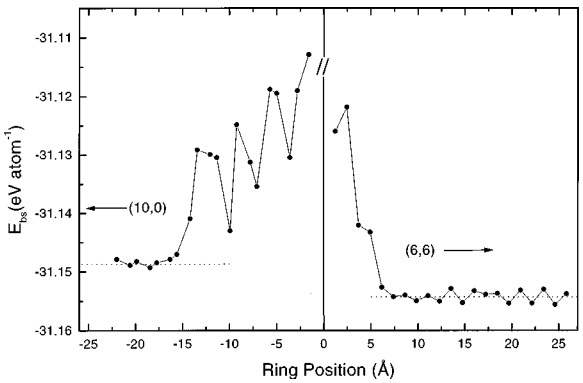

FIG. 5. Local variation of the electronic energy along the (10,0)/(6,6) junction. The computed energies are averaged on rings of 10 (respectively, 12) atomic sites for (10,0) [respectively, (6,6)] tubules. A continuous curve has been drawn between the points to guide the eyes.

B. Structural energy of the defect from the Tersoff potential

The force-field potential allows us to obtain a rapid measure of the structural energy cost of a single bent nanotube, working along the same way as for the band structure energy. Numerical results are given in Table I. The five junctions with opposite pentagon and heptagon have roughly the same energy, around 2.5 eV above that of the isolated, defect-free nanotubes. The energy is lower for the last two systems, where the odd-membered rings are adjacent. This result indicates that, with a local-energy model such as Tersoff's description, the energy cost introduced by the pentagon and heptagon is mostly located in the immediate neighborhood of these defects, and the perturbation is smaller when these two defects are joined. This result is in contrast with the relatively long range of the electronic energy associated with the defect illustrated in Fig. 5.

V. CONCLUSIONS

Several junctions between carbon nanotubes based on the pentagon-heptagon construction have been realized. The atomic structure of each system was optimized with the interatomic potential of Borštnik *et al.*, and further refined with the Tersoff potential using the Brenner parametrization. These calculations show that diametrically opposed pentagons and heptagons bend the structure at an angle around 36°. For instance, the (9,0)/(5,5) and (18,0)/(10,10) homologous junctions have the same bending angle and can therefore be nested inside one another to make a bilayer kneed nanotube, with the required 3.4 Å distance between the layers. The bend angle is reduced to 12° in the (8,0)/(7,1) joint where the pentagon and heptagon are adjacent.

Treating the half nanotubes as semi-infinite, local densities of states were determined along the joints with a tight-binding Hamiltonian that incorporates both σ and π electrons. This description improves earlier calculations of the π-electron DOS carried out for a few of the systems consid-

ered here. Quasioscillations of the local DOS with a triple period around the Fermi level was found in the metallic part of the (20,0)/(12,12) metal-semiconductor hybrid, very much as in the (10,0)/(6,6) junction. With the Tersoff potential, the excess of energy of the junction above that of the two half nanotubes is significantly smaller when the pentagon-heptagon is adjacent. No such trends could be deduced from the electronic contribution of the pentagon-heptagon defect energy, the averaged value of which was found to be 5.9 eV.

ACKNOWLEDGMENTS

This work was performed under the auspices of the interuniversity research program on Reduced Dimensionality Systems (Grant No. PAI-IUAP N. P4/10) initiated by the Belgian Federal OSTC. V.M. acknowledges a grant from the Belgian Fund for Industrial and Agricultural Research (FRIA). The authors acknowledge helpful discussions with J.C. Charlier, P. Lauginie, and J. Conard.

[1] R. F. Service, Science **271**, 1232 (1996).
[2] M. Dresselhaus, Phys. World **9**, 18 (1996).
[3] S. J. Tans, M. H. Devoret, H. Dai, A. Thess, R. E. Smalley, L. J. Geerligs, and C. Dekker, Nature (London) **386**, 474 (1997).
[4] M. Bockrath, D. H. Cobden, P. L. McEuen, N. G. Chopra, A. Zettl, A. Thess, and R. E. Smallet, Science **275**, 1922 (1997).
[5] Ph. Lambin, A. Fonseca, J. P. Vigneron, J. B. Nagy, and A. A. Lucas, Chem. Phys. Lett. **245**, 85 (1995).
[6] L. Chico, V. H. Crespi, L. X. Benedict, S. G. Louie, and M. L. Cohen, Phys. Rev. Lett. **76**, 971 (1996).
[7] R. Saito, G. Dresselhaus, and M. S. Dresselhaus, Phys. Rev. B **53**, 2044 (1996).
[8] J. C. Charlier, T. W. Ebbesen, and Ph. Lambin, Phys. Rev. B **53**, 11 108 (1996).
[9] X. Blase, J. C. Charlier, A. De Vita, and R. Car, Appl. Phys. Lett. **70**, 197 (1997).
[10] R. Tamura and M. Tsukada, Phys. Rev. B **55**, 4991 (1997).
[11] J. W. Mintmire, B. I. Dunlap, and C. T. White, Phys. Rev. Lett. **68**, 631 (1992).
[12] N. Hamada, S. I. Sawada, and A. Oshiyama, Phys. Rev. Lett. **68**, 1579 (1992).
[13] R. Saito, M. Fujita, G. Dresselhaus, and M. S. Dresselhaus, Appl. Phys. Lett. **60**, 2204 (1992).
[14] B. I. Dunlap, Phys. Rev. B **49**, 5643 (1994).
[15] P. Lauginie and J. Conard, J. Phys. Chem. Solids (to be published).
[16] S. Itoh, S. Ihara, and J. Kitami, Phys. Rev. B **47**, 1703 (1993).
[17] S. Ihara, S. Itoh, and J. I. Kitakami, Phys. Rev. B **48**, 5643 (1993).
[18] H. Terrones, M. Terrones, and W. K. Hsu, Chem. Soc. Rev. **24**, 341 (1995).
[19] D. L. Carroll, P. Redlich, P. M. Ajayan, J. C. Charlier, X. Blase, A. De Vita, and R. Car, Phys. Rev. Lett. **78**, 2811 (1997).
[20] S. Iijima, T. Ichihashi, and Y. Ando, Nature (London) **356**, 776 (1992).
[21] V. Ivanov, J. B. Nagy, Ph. Lambin, A. A. Lucas, X. B. Zhang, X. F. Zhang, D. Bernaerts, G. Van Tendeloo, S. Amelinckx, and J. Van Landuyt, Chem. Phys. Lett. **223**, 329 (1994).
[22] D. Bernaerts, X. B. Zhang, X. F. Zhang, S. Amelinckx, G. Van Tendeloo, J. Van Landuyt, V. Ivanov, and J. B. Nagy, Philos. Mag. A **71**, 605 (1995).
[23] X. F. Zhang and Z. Zhang, Phys. Rev. B **52**, 5313 (1995).
[24] X. B. Zhang, X. F. Zhang, D. Bernaerts, G. Van Tendeloo, S. Amelinckx, J. Van Landuyt, V. Ivanov, J. B. Nagy, Ph. Lambin, and A. A. Lucas, Europhys. Lett. **27**, 141 (1994).
[25] B. I. Dunlap, Phys. Rev. B **50**, 8134 (1994).
[26] B. Borštnik and D. Lukman, Fullerene Sci. Technol. **2**, 357 (1994).
[27] D. W. Brenner, Phys. Rev. B **42**, 9458 (1990).
[28] Ph. Lambin, A. Fonseca, J. B. Nagy, and A. A. Lucas, Synth. Met. **77**, 249 (1996).
[29] J. Tersoff, Phys. Rev. B **39**, 5566 (1989).
[30] A. Fonseca, E. A. Perpète, P. Galet, B. Champagne, J. B. Nagy, J. M. André, Ph. Lambin, and A. A. Lucas, J. Phys. B **29**, 4915 (1996).
[31] M. Terrones and H. Terrones, Fullerene Sci. Technol. **4**, 517 (1996).
[32] J. C. Slater and G. F. Koster, Phys. Rev. **94**, 1498 (1954).
[33] J. C. Charlier, X. Gonze, and J. P. Michenaud, Phys. Rev. B **43**, 4579 (1991).
[34] R. Haydock, V. Heine, and M. J. Kelly, J. Phys. C **8**, 2591 (1975).
[35] J. W. Mintmire and C. T. White, Carbon **33**, 893 (1995).
[36] E. Heilbronner and H. Bock, *The HMO-Model and its Application: Basis and Manipulation* (Wiley, London, 1976), p. 20.